Received: 26 September 2019 | Revised: 26 June 2020 | Accepted: 16 July 2020

DOI: 10.1096/fj.201902462RR

RESEARCH ARTICLE

THE FASEB JOURNAL

Noncanonical function of long myosin light chain kinase in increasing ER-PM junctions and augmentation of SOCE

Nityanand Srivastava[1] | Mohammad Tauseef[1,2] | Ruhul Amin[1] | Bhagwati Joshi[1] | Jagdish Chandra Joshi[1] | Vidisha Kini[1] | Jennifer Klomp[1] | Weenan Li[3] | Nebojsa Knezevic[1] | Nicolas Barbera[4] | Shahid Siddiqui[1] | Alexander Obukhov[3] | Andrei Karginov[1] | Irena Levitan[4] | Yulia Komarova[1] | Dolly Mehta[1,2]

[1]Department of Pharmacology and Center for Lung and Vascular Biology, The University of Illinois, College of Medicine, Chicago, IL, USA

[2]Department of Pharmaceutical Sciences, Chicago State University College of Pharmacy, Chicago, IL, USA

[3]Department of Cellular and Integrative Physiology, Indiana University School of Medicine, Indianapolis, IN, USA

[4]Department of Medicine, The Uniiversity of Illinois, Chicago, IL, USA

Correspondence
Dolly Mehta, Department of Pharmacology,The University of Illinois, College of Medicine, 835 S. Wolcott Avenue, Chicago, IL 60612, USA.
Email: dmehta@uic.edu

Funding information
NIH| National Heart, Lung, and Blood Institute (NHLBI), Grant/Award Number: HL84153, HL137179-01, PO1-HL60678 and HL077806

Abstract

Increased endothelial permeability leads to excessive exudation of plasma proteins and leukocytes in the interstitium, which characterizes several vascular diseases including acute lung injury. The myosin light chain kinase long (MYLK-L) isoform is canonically known to regulate the endothelial permeability by phosphorylating myosin light chain (MLC-P). Compared to the short MYLK isoform, MYLK-L contains an additional stretch of ~919 amino acid at the N-terminus of unknown function. We show that thapsigargin and thrombin-induced SOCE was markedly reduced in *Mylk-L*$^{-/-}$ endothelial cells (EC) or MYLK-L-depleted human EC. These agonists also failed to increase endothelial permeability in MYLK-L-depleted EC and *Mylk-L*$^{-/-}$ lungs, thus demonstrating the novel role of MYLK-L-induced SOCE in increasing vascular permeability. MYLK-L augmented SOCE by increasing endoplasmic reticulum (ER)-plasma membrane (PM) junctions and STIM1 translocation to these junctions. Transduction of N-MYLK domain (amino acids 1-919 devoid of catalytic activity) into *Mylk-L*$^{-/-}$ EC rescued SOCE to the level seen in control EC in a STIM1-dependent manner. N-MYLK-induced SOCE augmented endothelial permeability without MLC-P via an actin-binding motif, DVRGLL. Liposomal-mediated delivery of N-MYLK mutant but not ΔDVRGLL-N-MYLK mutant in *Mylk-L*$^{-/-}$ mice rescued vascular permeability increase in response to endotoxin, indicating that targeting of DVRGLL motif within MYLK-L may limit SOCE-induced vascular hyperpermeability.

KEYWORDS

endoplasmic reticulum-plasma membrane junctions, long myosin light chain kinase, store-operated calcium entry, stromal interacting molecule 1, vascular permeability

Abbreviations: ALI, acute lung injury; EC, endothelial cells; ER-PM junctions, endoplasmic reticulum-plasma membrane junctions; Esyt-3, extended synaptogamin-3; HPAEC, human pulmonary arterial endothelial cells; HUVEC, human umbilical vascular endothelial cells; LPS, lipopolysaccharide; MAPPER, membrane-attached peripheral ER; MLC, myosin light chain; MYLK-L, long myosin light chain kinase ; SNP, single nucleotide polymorphism; SOCE, store-operated calcium entry; STIM1, stromal interacting molecule 1; TIRFM, total internal reflection fluorescence microscopy.

Nityanand Srivastava andMohammad Tauseef contributed equally to this study.

1 | INTRODUCTION

Vascular endothelium has the pivotal task of dynamically restricting the passage of macromolecules and inflammatory cells to underlying tissue in order to maintain tissue homeostasis. Permeability increasing mediators disrupt the endothelial barrier function in part by inducing phosphorylating myosin light chains (MLC) which in turn trigger actin-myosin-mediated endothelial contraction.[1-3] Increased endothelial permeability can lead to excessive exudation of plasma proteins and leukocytes in the interstitium, the hallmark of several vascular diseases including acute respiratory distress syndrome, ischemia/reperfusion injury, and atherosclerosis.[4-7]

Myosin light chain kinase1 (MYLK1) gene encodes short (108-130 kDa) and long (~220 kDa) isoforms of MYLK which phosphorylate MLC.[8-10] MYLK-L is expressed in various non-muscle cells including endothelial cells (EC) and regulates the endothelial permeability in response to permeability increasing mediators such as thrombin or LPS.[5,11-16] Hence, mice lacking MYLK-L globally were protected from several vascular diseases such as sepsis, acute lung injury (ALI), and atherosclerosis.[6,16-19] However, Tie2-Cre-mediated deletion of MYLK-L in endothelium of the mice failed to suppress LPS-induced lung vascular hyperpermeability.[20] These findings indicate that MYLK-L may have a complex role in regulating the vascular permeability.

Structurally, MYLK-L contains all the domains that are present in the short smooth muscle MYLK isoform, but in addition, has a unique stretch of ~919-amino acid N-terminal domain that contains consensus sites for phosphorylation by multiple protein kinases,[2,8,9,18,21] as well as additional actin-binding domains.[22,23] N-terminal domain of MYLK-L also contains the sites for genetic variations known as single-nucleotide polymorphism (SNP) that are associated with the vascular diseases.[24-26] Surprisingly, studies to date have mostly focused on MYLK-L induction of MLC phosphorylation as the primary permeability-increasing process in EC, while the unique role of the N-terminal domain of MYLK-L in regulating the endothelial permeability remains largely unexplored.

An increase in intracellular Ca^{2+} is required for the activation of diverse signaling pathways including activation of the MYLK activity that culminate in the disruption of the endothelial barrier.[2,27-30] Permeability-increasing agonists increase intracellular Ca^{2+} by depleting the endoplasmic reticulum (ER) store, followed by Ca^{2+} entry through plasma membrane (PM) channels referred to as store-operated Ca^{2+} entry (SOCE).[29,31-34] Stromal interaction molecule 1 (STIM1) senses Ca^{2+} gradients in the ER[27,35-37] and assembles into higher-order oligomers known as puncta upon ER-Ca^{2+} depletion. These puncta are formed at discrete sites called ER-PM junctions where STIM1 interacts with plasmalemmal Ca^{2+} channels such as Orai1/TRPC1 to activate SOCE.[35,38,39] Evidence also links MYLK-L to modulation of Ca^{2+} entry but the mechanisms remain largely unknown.[40] In this study, we demonstrate that the MYLK-L through its N-terminal domain mediates SOCE which then induces vascular hyperpermeability. This domain stabilizes ER-PM junctions and SOCE through DVRGLL motif independent of MYLK-L catalytic activity. Our findings established previously unknown role of the N-MYLK-DVRGLL motif in inducing lung edema formation in response to the endotoxin, LPS. Disruption of this domain in MYLK-L may be regarded as a therapeutic approach to limit the SOCE-mediated increase in endothelial permeability in ALI.

2 | MATERIALS AND METHODS

2.1 | Materials

Human Pulmonary endothelial cells (HPAEC) (Cat. No. CC-2585), Human Umbilical Vascular endothelial cells (HUVEC) (Cat. No. C2517A), endothelial growth medium (EBM-2) (Cat. No. CC-3162), nucleofector kit (Cat. No. VPB-1002), and electroporation system were obtained from Lonza, Allendale, NJ, USA. FuGENE (Cat. No. E2311). FuGENE transfection reagent was procured from Promega, Madison, WI 53711 USA. Anti-Alexa Fluor 568 and −488, CD45.1 (clone 30F11) (Cat. No. 11-0451), and Actin (BA3R) (Cat. No. MA5-15739) antibodies were obtained from Thermo Fisher, Waltham, MA, USA. CD31 (Cat. No. 102410) anti-body was procured from BioLegend, San Diego, CA, USA. Anti-MYLK antibodies A-10 (Cat. No. SC-515020), which recognizes N-terminus of MYLK-L and A8, which recognizes both long and short isoforms of MYLK (Cat. No. SC- 365352), respectively, were from Santa Cruz Biotechnology, Dallas, TX, USA. Protein A-HRP was from Milipore Sigma (Cat. No,18-160). Anti-STIM1 (Cat. No. 4916; Cat. No. sc-79106) and anti-GFP (Cat. No. SC- 9996; D4.1Cat. No. 2956S) antibodies were from Santa Cruz Biotechnology or Cell Signaling, Danvers, MA, USA. Thapsigargin (Cat. No. 586005), was purchased from EMD Millipore, MA, USA. Thrombin (Cat. No. T4393), collagenase (Cat. No. 10103578001), and Lipopolysaccharide (Cat. No. 2880, 2630) were purchased from Sigma Aldrich, St. Louis, MO 63178, USA. Fura 2-AM (Cat. No. F1221), Prolong gold anti-fade (Cat. No. P36934) and Dyna beads (Cat. No. 11155D) were purchased from Invitrogen, Carlsbad, CA, USA. Paraformaldehyde was purchased from Fisher Scientific, Hampton, NH, USA. Scrambled (Cat. No. D-001810-01-05) and MYLK siRNA were custom made from Dharmacon, Lafayette, CO, USA.

2.2 | Experimental animals

Animal studies were approved by the Institutional Animal Care and Use Committee (IACUC) of University of Illinois (UIC). *Mylk-L*$^{-/-}$ mice breeding pair in a C57Blk/6J background was obtained from M. Watterson (Northwestern University, Chicago, IL).[17] Mice colonies were maintained at pathogen-free animal housing facility at the University of Illinois at Chicago (UIC). C57Blk/6J mice initially acquired from The Jackson Laboratory and bred at UIC were used as wild-type (WT) controls. All experiments were performed on 8- to 10-week-old mice.

2.3 | Fluorescence-activated cell sorting

Mice transducing indicated cDNA were euthanized after 48 hours of transduction, followed by exposure of the thoracic cavity. Five milliliter of cold PBS was then injected via the right ventricle to flush the blood from the lungs. Lung tissues were minced and enzymatically digested with 1 mg/mL collagenase A (Roche, New York, NY) for 50 minutes at 37°C. Digested tissue was passed through a 75-μm nylon filter to obtain single-cell suspensions. The red blood cells were lysed, and cell suspension was washed with FACS buffer. Cells were re-suspended in one milliliter of FACS buffer and incubated with Fc blocking antibody for 10 minutes, to prevent binding of nonspecific FcγRIII/II. Cells were then labeled with indicated anti-mouse antibodies (as a cocktail of 1:100 dilution of anti-CD31, and anti-CD45), for 1 hour on ice. Samples were washed and resuspended in FACS buffer to a concentration of one million cells/mL and sorted.[28] Sorted cells lysates were then immunoblotted using anti-GFP antibody to determine the level of protein expression.

2.4 | Cell culture

HPAEC and HUVEC were cultured in complete EBM2 medium in a T-75 flask coated with 0.1% gelatin and supplemented with 10% fetal bovine serum (FBS). Cells were maintained at 37°C in a humidified atmosphere of 5% CO_2 and 95% air until they formed a confluent monolayer.[41] Cells were detached using 0.05% Trypsin containing 0.02% EDTA and plated on 100 mm dishes. Mouse lung endothelial cells (MLECs) were isolated as described.[28] Briefly, blood-free mouse lungs were minced, digested with collagenase at 37°C for 45 minutes, triturated, and centrifuged at 3000 rpm. Cell suspension was incubated with PECAM-1-coated Dyna beads for an hour after which ECs were magnetically sorted. Isolated EC were plated on fibronectin coated T-25 flask and cultured with DMEM containing endothelial growth supplement till confluent. EC were detached using 0.05% Trypsin containing 0.02% EDTA and plated on coverslips or dishes as required for experiments.

2.5 | Generation of constructs

A full length GFP-tagged mouse MYLK-L (WT-MYLK-L) plasmid was generously provided by Dr. Patricia Gallagher (School of Medicine, Indiana University).[10] Other constructs, m-cherry-STIM1; YFP-MAPPER and YFP-ESYT-3 were provided by Dr. Jen Liou, Department of Physiology, University of Texas Southwestern Medical Center, Dallas, TX,[35,42,43] FL-MYLK plasmid was cloned into EYFP vector. To do so, PCR primers were designed to amplify YFP from YFP plasmid, pYFP-C1, cat #632524, Clontech, with flanking restriction sites, 5′- AgeI and 3′- NotI. The PCR fragment was digested with 5′- AgeI and 3′- NotI. The vector. The digested PCR fragment was then ligated to the digested vector. N-MYLK; C-MYLK; ΔDVRGLL-N-MYLK, ΔDVRGLL-DFRDLL-N-MYLK, and FL-MYLK-ΔDVRGLL mutants were generated from full-length MYLK cDNA using the following PCR primers: 5′-GACGACC TGAAGGACATCCCAGCCGAGCAG-3′ MYLKL-end -N-terminal-F and 5′-CTGCTCGGCTGGGATGTCCTT CAGGTCGTC-3′ MYLKL-end -N-terminal-R; 5′- ATT ACATCTAGATCACTCCTCCTCCTCCTC-3′ MYLKL-end -C-terminal-F and 5′- ATTACAGGTACCATGGA TTTCCGCGCCAAC-3′ MYLKL-end -C-terminal-R; 5′- CCGTCTCTTTTCTCCGTCTTCCTCCTC-3′ hMYLKL-end -N-terminal-delDVRGLL-F and 5′-GACGGAGAAAAGAGACGGGTGGAGACC-3′ hMYLKL-end -N-terminal-DELDVRGLL-R; 5′- GGG CAGCTGGGAAAGAAGGTGAGCACCAAGACC-3′ hMYLKL-end -N-terminal-delDFRDLL-F sub cloned into pEGFP-N1 vector from Clontech via. Briefly, PCR primers were designed with flanking restriction sites, 5′-XhoI and 3′-BamHI, to amplify the full length Orai1. The PCR fragment was then digested 5′- XhoI and 3′- BamHI and ligated to the vector pAmCyan-N1 also digested at the same sites 5′- XhoI and 3′- BamHI. In the primers, the bold and italicized base pairs indicated restriction sites while the underlined base pairs indicated the mutated amino acid. The final PCR product "c" was then digested with XhoI and BamHI and ligated to pEYFP-N1 vector also digested with the same restriction enzymes to generate the resulting plasmid pEYFP-N1-STIM1mutants. The ligated reactions were transformed into DH5α Subcloning Effiency Competent Cells (Thermo Fisher Scientific, Grand Island, NY). The transformed cells were plated onto LB plates supplemented with 25 μg/mL Kanamycin (Thermo Fisher). After overnight incubation at 37°C, single colonies were cultured in LB with 25 μg/mL Kanamycin overnight. Plasmid DNA was obtained using GeneJet Plasmid Miniprep kit (Thermo Fisher Scientific) and

analyzed by restriction digestion to confirm the correct size of the vector (pEYFP-N1) and insert (MYLK). Further amplification of the plasmid DNA was done using NucleoBond Xtra Midi Kit (Clontech Laboratories, Mountain View, CA). The resulting plasmid was verified for DNA purity and identity by DNA quantification, gel analysis, and sequencing analysis.

2.6 | MYLK-L siRNA

Three sequences between nucleotides 1428 and 1634 was custom designed to target MYLK-L expression. Target sequence #1; NNGGACUGCGCUGUUAUUGA; #2; NNGUGGAAAGGGCUUGCCGUGA; #3; and NNUGGGCAGCCACUCCAGUAC. Sequence #3 was found to deplete maximally MYLK-L and was used as the MYLK-L siRNA for remaining study.

2.7 | Transfection of cells

Transfection of cDNA in HPAEC, HUVEC or mouse EC were done as described previously using FuGene (Promega) or Amaxa electroporation (Lonza).[28,41,44] cDNA (50 ng) or 25 nM siRNAs were transfected into HPAEC or HUVEC. In experiments requiring co-transfection with siRNAs as well with cDNA, siRNA were transduced using Santacruz transfection reagent or Amaxa electroporation and after 24 hours cells were transfected with cDNA using FuGENE transfection reagents according to the manufacturer's protocol. Confluent monolayers were incubated in EBM2 basal medium supplemented with 0.1% FBS for 1 hour before stimulation with thapsigargin or thrombin. HPAEC were used between passages 5 and 7.

2.8 | Cytosolic Ca^{2+} measurements

An increase in intracellular Ca^{2+} was measured using the Ca^{2+}-sensitive fluorescent dye Fura 2-AM as described.[28,44] Briefly, HPAE or mouse lung EC were transfected with indicated constructs for 24 hours or siRNA for 48 hours, respectively. After respective transfection times, cells were serum deprived for 1 hour. They were then loaded with Fura 2-AM dye for 20 minutes, rinsed three times with Ca^{2+} free HBSS media and placed on the stage of an Axiovert 35 microscope (Carl Zeiss MicroImaging, Inc) equipped with a 40× plan-Neofluar objective (NA 1.30 oil). Only YFP transfected cells were selected for Ca^{2+} measurement. In each experiment, at least 4-5 YFP-tagged cells were imaged for Ca^{2+} analysis.

2.9 | Immunoblotting

Cell or lung tissue were lysed in modified radioimmunoprecipitation buffer (50 mM Tris, pH 7.4, 1% deoxycholic acid, 150 mM NaCl, 0.25 mM EDTA, pH 8.0, 0.5% Nonidet P-40, 0.1% SDS, 1 mM NaF, 1 mM sodium orthovanadate,1 mM phenylmethylsulfonyl fluoride, and 2 g/mL of (leupeptin, aprotinin, and pepstatin A) on ice for 20 minutes. In some experiments cell lysates were directly prepared using Laemmli buffer.

For assessing MYLK fragmentation following LPS-induced lung injury, WT, or MYLK null lungs obtained without or with LPS were homogenized in RIPA buffer. Lysates containing equal amounts of protein were then treated with DTT (10 mM) and mercaptoethanol supplemented in 2X Laemmli buffer. Membranes were immunoblotted with MYLK antibody raised against N-terminus (A10) followed by Protein A-HRP secondary antibody.

2.10 | Assessment of STIM1 puncta formation and ER-PM junctions

Cells were electroporated with control or MYLK-L siRNA along with YFP-STIM1 or GFP-MAPPER or ESYT3-GFP cDNA and seeded on 35 mm glass bottom dishes (Nunc) as described.[44] After 48 hours post transfection, cells were serum starved in basal media supplemented with 0.1% FBS for 1 hour followed by rinsing with PBS. Images were taken first in Ca^{2+} containing buffer followed by Ca^{2+} and Mg^{2+} free buffer. After few images, cells were treated with 2 μM thapsigargin and imaged every 5 seconds for 20 to 30 cycles at 37°C. All confocal images were obtained with a pinhole setting of 1 Airy Unit using a Zeiss LSM 880 inverted laser scanning system equipped with a heated stage (Warner Instruments), Plan-Apochromat 63×/1.4 NA oil immersion objective, an Argon (λ = 458, 488, 514 nm) and diode-pumped solid-state laser (λ = 561 nm), two photomultiplier tubes, and Gallium arsenide phosphide detector. For EYFP-Stim1, 488 nm or 514 nm illumination was provided by an Argon laser and emission was selected with a 530-600 nm bandpass filter.

TIRF (total internal reflection fluorescence) microscopy was performed using an CFI Apo TIRF 100×/1.49 objective on a spinning-disk confocal and TIRF system built around a Ti-E Perfect Focus microscope (Zeiss) with an HQ2 camera and an EM camera (c9100-13; Hamamatsu) controlled by Micro-Manager software.[45] Images were acquired every 5 seconds for 20-30 cycle after thapsigargin stimulation.

To determine GFP-STIM1 or GFP-MAPPER or GFP-ESYT3 puncta, images of cells expressing GFP was background subtracted and subjected to Fourier transformation

with a high-pass filter to create binary-like images. The transformed images were subjected to threshold analysis to obtain the total number of puncta.

2.11 | Assessment of lung vascular permeability

Mice were exposed to nebulized LPS. Lung edema and Evans blue-conjugated albumin (EBA) (20 mg/kg) influx across lung parenchyma were determined as indices of vascular permeability, as described previously.[28,29,44] Briefly, EBA (20 mg/kg) was injected retro-orbitally 30 minutes before euthanizing the mice. Blood was obtained from the right ventricle of the heart into heparinized syringes, and plasma was separated. Lungs were homogenized. Lung lysates and plasma were incubated with two volumes of formamide for 18 hours at 55 to 60°C, then centrifuged at 5000 *g* for 30 minutes. The optical density of the supernatant was determined spectrophotometrically at 620 nm (Evans blue) and 740 nm (hemoglobin correction). EBA extravasation was calculated as EBA influx in lung vs that in plasma. For lung edema formation, left lungs from the same mice used for Evans blue albumin extravasation were excised and completely dried in a 60°C oven overnight for calculation of lung wet-dry ratio.

2.12 | Liposomal delivery of cDNA for rescue experiments

Cationic liposomes were made using a mixture of dimethyldioctadecyl-ammonium bromide and cholesterol in chloroform, as described previously.[28,41,44] Vector or indicated MYLK-cDNA (50 μg) were mixed with 100 μl of liposomes. Liposomes encapsulating cDNA were injected into mouse vasculature via retroorbital injection. After 48 hours, mouse lungs were used for determining lung vascular permeability. EC from lungs receiving cDNA were sorted as above to assess the expression of MYLK.

2.13 | Image processing and data analysis

The 16-bit images were analyzed with and morphometric data were obtained using Fiji (Image J; National Institutes of Health) image-processing software, and results were assessed for statistical significance by two-way ANOVA with Bonferroni test (for mean ± SD). Automated identification of GFP-STIM1, GFP-MAPPER, and GFP-ESYT3 puncta was performed using ImageJ 1.49. Individual images were converted into 8-bit and puncta were identified by a threshold set via a mixture model, to create a mask image. Using the mask images, the number of STIM1-GFP, GFP-MAPPER, and GFP-ESYT3 puncta were scored with automatic "Analyze Particles" algorithm of ImageJ software and using cluster size of 3-100 pixels and circularity 1.0-3.0. The data were expressed as the number of puncta per cell and the size range was set to ~0.5× to 2× the area of selected puncta. An individual data point were performed using GraphPad Prism 6.

2.14 | Statistical analysis

Statistical differences among groups were assessed using a one-way ANOVA followed by paired two tailed *t* test. A value of $P < .05$ was considered statistically significant.

3 | RESULTS

3.1 | MYLK-L increases vascular permeability by controlling store-operated Ca^{2+} entry (SOCE)

We first addressed the possible role of MYLK-L in regulating SOCE in EC. We sorted EC from WT and MYLK-L null lungs and using antibody raised against N-terminus of MYLK , confirmed that fresh endothelium of WT lungs expresses long isoform of MYLK (MYLK-210) (Figure S1A). This form was not visible in EC from *Mylk-L*$^{-/-}$ lungs (Figure S1A). Fura2-labeled EC were stimulated with thrombin which depletes the ER Ca^{2+} store via the protease activating receptor 1 (PAR1)-phospholipase C pathway.[29,31,44] For comparison, we used thapsigargin to deplete the ER Ca^{2+} store and induce SOCE independent of activation of ligand-coupled receptors or second messenger systems.[29,31,46] We observed that, under Ca^{2+}-free bath conditions, EC isolated from lungs of either WT or *Mylk-L*$^{-/-}$ mice showed a similar increase in intracellular Ca^{2+}due to ER Ca^{2+} release in response to either thrombin or thapsigargin (Figure 1A-D). However, loss of MYLK-L significantly reduced Ca^{2+} entry induced upon re-addition of Ca^{2+} (Figure 1A-D). This function of MYLK-L was specific to SOCE because stimulation of EC with OAG, a cell-permeable analog of DAG that activates receptor operated Ca^{2+} channels (ROC),[28,47,48] induced Ca^{2+} entry to the same extent in both WT and MYLK-L deficient ECs (Figure S1B,C).

To further corroborate the role of MYLK-L in regulating SOCE, we depleted MYLK-L in HPAEC using siRNA and stimulated them with thrombin or thapsigargin. In these experiments, a unique 207-base pair sequence between nucleotides 1428 and 1634, was used to design a MYLK-L-specific targeting siRNA. Sequence "C" was most effective in depleting MYLK-L (Figure S1D). Immunoblotting with anti-MYLK antibody which recognize both long and short isoforms of MYLK further confirmed that MYLK-L siRNA

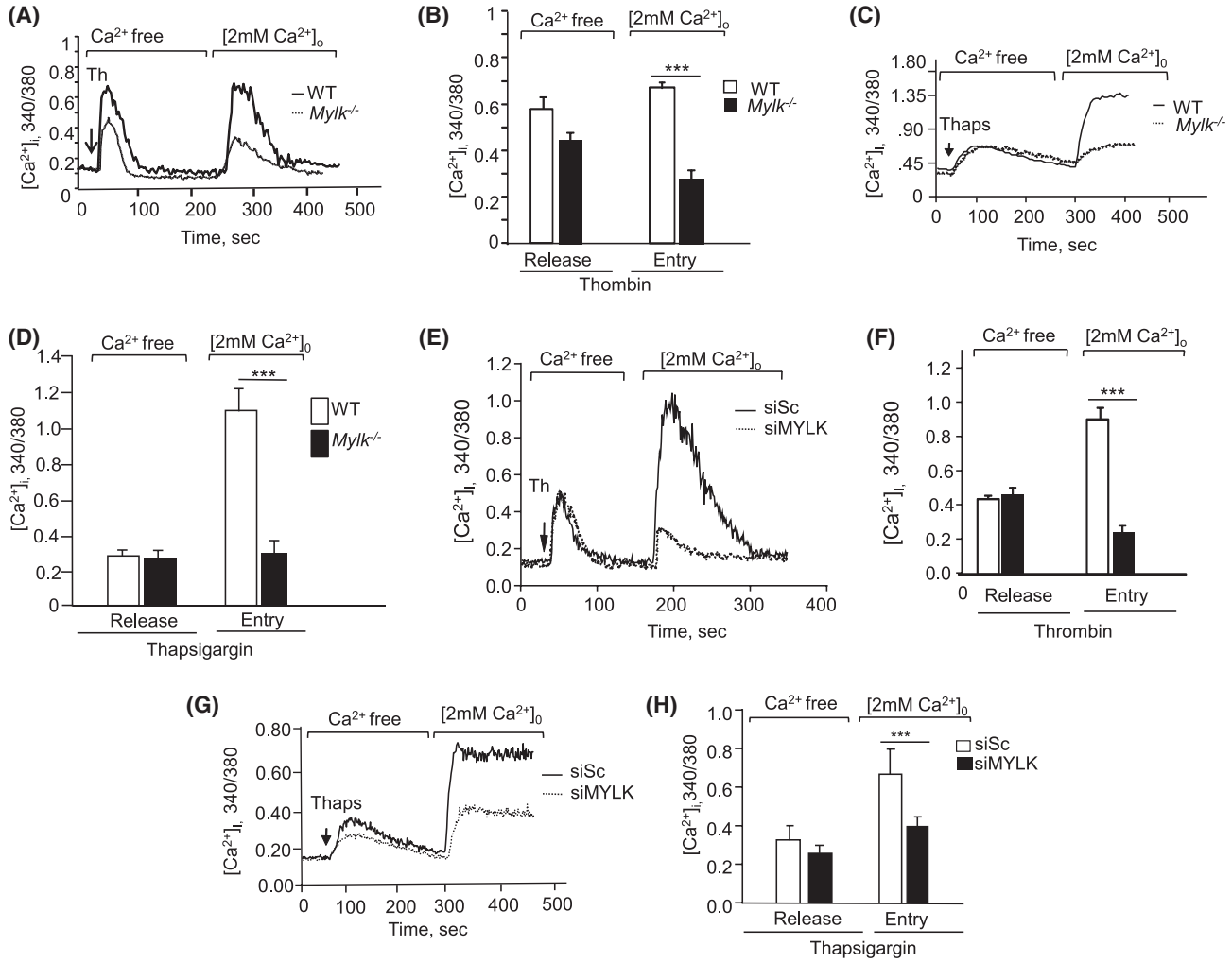

FIGURE 1 MYLK-L augments store-operated Ca^{2+} entry. A-E, Changes in intracellular Ca^{2+} concentration in response to thrombin (A-B) or thapsigargin (C-D) in EC isolated from WT or *Mylk-l*$^{-/-}$ lungs. The representative Fura2-AM 340/380 traces in A and C shows a mean Ca^{2+} response from 10-15 EC within a single experiment. Plots in B and D shows mean ± SD of changes in intracellular Ca^{2+} as reflected by 340:380 ratio from 3-4 individual experiments. ***, $P < .001$ compared to thrombin or thapsigargin stimulated MYLK-L null EC following re-addition of 2 mM Ca^{2+}. E-H, HPAEC were transfected with scrambled or MYLK-L "C" siRNA and changes in intracellular Ca^{2+} concentration was determined in control or MYLK-L-depleted HPAECs following 50 nM thrombin (E-F) or 2 μM thapsigargin (G-H) stimulation. The representative Fura2-AM 340/380 traces are shown in panels E and G while F and J depict a mean Ca^{2+} response from 10-15 ECs in a field within a single experiment. Plots (F and H) shows mean ± SD of changes in intracellular Ca^{2+} from 3-4 individual experiments ***, $P < .001$ compared to thrombin or thapsigargin stimulated MYLK-L-depleted (siMYLK) EC following re-addition of 2 mM Ca^{2+}.

depleted 220 kDa MYLK-L isoform but not the other MYLK isoforms (Figure S1E). Like mouse EC, depletion of MYLK-L in human EC suppressed SOCE (Figure 1E-H), suggesting that MYLK-L is required for full activation of SOCE.

As SOCE-induced increase in intracellular Ca^{2+} leads to microvascular hyperpermeability,[29,31,44,49,50] we determined the role of MYLK-L-regulated SOCE in increasing vascular permeability. Thus, we treated WT or MYLK-L null mice with PAR1 agonist peptide or thapsigargin and determined wet-dry lung ratio and albumin accumulation in the lungs. We found that both PAR1 peptide and thapsigargin significantly increased lung vascular permeability; however, this response was not observed in *Mylk-L*$^{-/-}$ lungs (Figures 2A,B and S1F). We also determined transendothelial electrical resistance (TEER) across endothelial monolayer in control and MYLK-L-depleted EC and found that MYLK-L-depleted EC showed markedly suppressed barrier dysfunction both by thrombin and thapsigargin (Figure 2C,D). Together, these findings demonstrate that MYLK-L-mediated SOCE activity contributes in increasing endothelial permeability.

3.2 | MYLK-L depletion impaired STIM1 puncta formation

STIM1 puncta formation is required to couple ER Ca^{2+} depletion with activation of SOCE channels such as Orai1 or TRPC1 at PM.[38,39,51] Therefore, we investigated whether

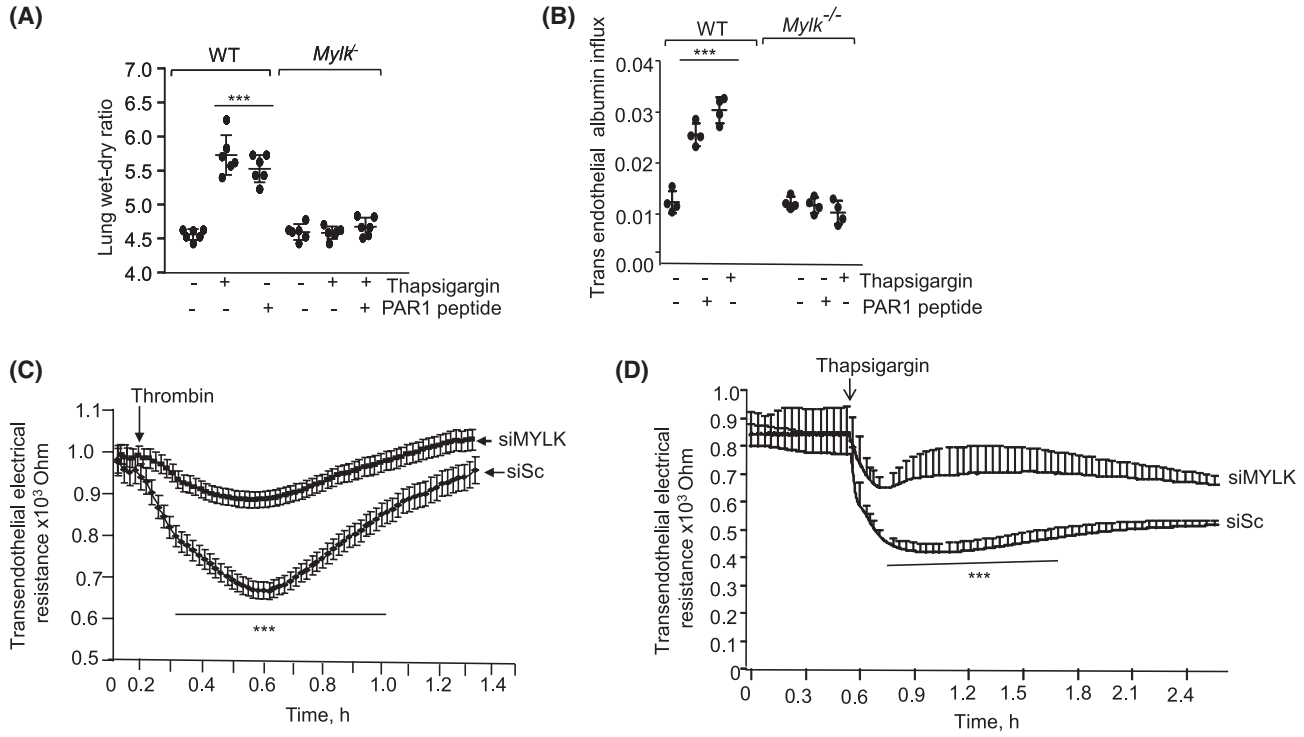

FIGURE 2 MYLK-L-induced store-operated Ca^{2+} entry increases endothelial permeability. A and B, WT or *Mylk-l*$^{-/-}$ mice received vehicle (-), PAR1 agonist peptide or thapsigargin (1 mg/kg body weight) *iv* and after 30 minutes lung edema (A) or transendothelial albumin was quantified. The plot shows individual values along with mean and SD. ***, $P < .001$ compared to vehicle injected WT mice and MYLK null mice after without or with indicated agonists injection. n = 4-6 mice per group. C and D, HPAECs seeded on gold-plated electrodes were transfected with scrambled or MYLK-L "C" siRNA and endothelial barrier function was determined by measuring transendothelial electrical resistance (TEER) in real time in naive monolayers following 50 nM thrombin (C) or 2 μM thapsigargin (D) stimulation. Plot shows mean ± SD of alteration in TEER from 3-4 individual experiments ***, $P < .001$ compared to MYLK-L-depleted (siMYLK) ECs.

MYLK-L regulated STIM1 puncta formation. For imaging studies, we used human umbilical vein EC (HUVEC) which have similar expression of MYLK as HPAEC (Figure S1G) but have higher transfection efficiency. We observed formation of STIM1 puncta at PM in control EC following thapsigargin stimulation (Figure 3A,B). Depletion of MYLK-L, however, markedly suppressed-induced STIM1 puncta formation (Figures 3A,B and S1H). Furthermore, these results were confirmed in experiments using TIRF microscopy (Figure 3C,D), a method allowing selective illumination of fluorescent probes within ~100 nm of the PM.[52] These results demonstrate that MYLK-L is required for formation or stabilization of STIM1 puncta. We, however, did not observe any differences in the expression levels of STIM1 and Orai1 in MYLK-L-depleted cells (Figure S1I).

3.3 | MYLK-L increases ER-PM junctions

Studies show that STIM1 accumulates at ER-PM junctions.[27,35] Therefore, we tested whether MYLK-L-induced STIM1 puncta formation via regulating ER-PM junctions. Using TIRF microscopy, we compared the number of ER-PM junctions in control and MYLK-L-depleted EC for both membrane-anchored peripheral ER marker known MAPPER, which selectively labels ER-PM junctions,[51,53] and the extended synaptogamin protein-3 (ESYT-3), which tethers the ER to the PM independent of ER depletion.[51,53,54] Interestingly, the numbers of both MAPPER- and E-SYT3-positive junctions were significantly reduced in MYLK-L-depleted ECs compared to control ECs under basal conditions (Figure 4A-D). Since MAPPER- and E-SYT3-positive ER-PM junctions were not increased after thapsigargin stimulation, that is, insensitive to ER Ca^{2+} concentration, we concluded that MYLK-L is required for stabilization of ER-PM junctions. Therefore, our data indicate that MYLK-L maximally activates SOCE by organizing STIM1 puncta at ER-PM junctions.

3.4 | MLCK-L augments SOCE through N-terminus

MYLK-L has an additional unique stretch of ~919 amino acid at the N-terminus not present in smooth or short MYLK isoform.[8,9,23] Thus, we sought to investigate whether MYLK-L regulated SOCE through this stretch. We generated two fragments of full-length MYLK-L (FL-MYLK), the N-terminus mutant containing amino acids 1-919 (hereafter, N-MYLK) and

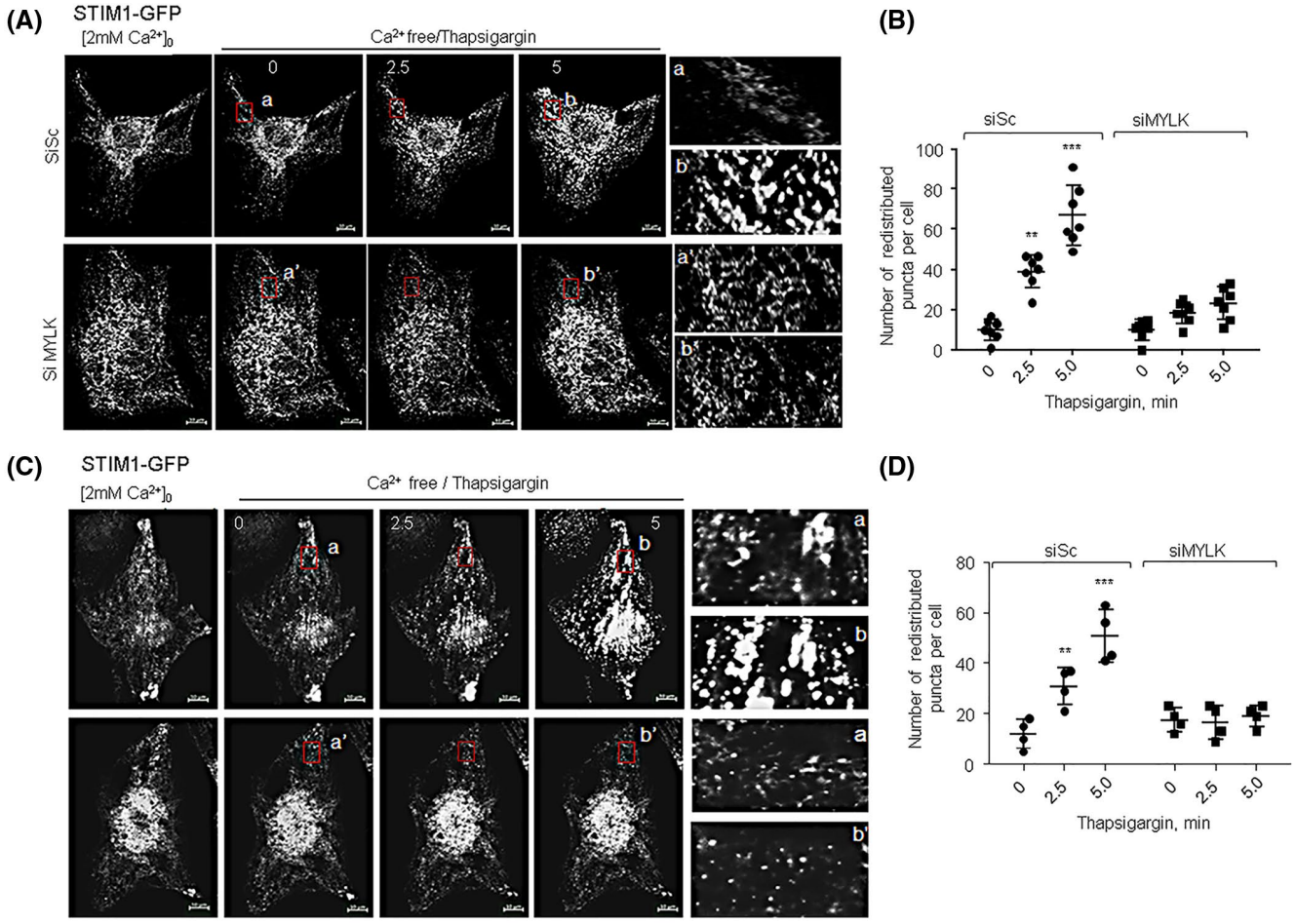

FIGURE 3 MYLK-L depletion impairs STIM1 puncta formation. A and B, Live-cell confocal images of STIM1-GFP expressed in control (SiSc) or MYLK-L-depleted (SiMYLK) HUVEC before and after different times (min, right corner) post thapsigargin challenge. Inserts show enlarged part of the cell. Panel A shows a representative image while B shows quantification of STIM1 puncta. C and D, Analysis of STIM1 puncta using TIRF live-cell images of STIM1-GFP expressed in control or MYLK-L-depleted HUVEC before and after different times (min, right corner) post thapsigargin challenge. Panel C shows a representative image while D shows quantification of STIM1 puncta. In A and C, the scale bar represents 10 μm. Plot shows mean ± SD of STIM1 puncta per cell from multiple cells (n > 5) from experiments that were repeated three times. **, $P < .01$ and ***, $P < .001$ compared to naïve siSc transfected ECs and naïve or stimulated MYLK-L-depleted EC.

the C-terminus mutant containing amino acids 920-1951 that is similar to smooth muscle (or short) MYLK isoform (hereinafter, C-MYLK), and determined their roles in promoting SOCE (Figure 5A). We found a marked amplification of SOCE activity in response to either thrombin or thapsigargin in EC overexpressing the N-MYLK mutant but not the C-MYLK mutant (Figures 5B-D and S2A,B). ECs overexpressing C-MYLK mutant exhibited marked kinase activity as evident from increased level of MLC phosphorylation compared to cells expressing N-MYLK mutant or FL-MYLK (Figure S2C). These data indicate that N-MYLK domain is necessary and enough to promote SOCE independent of kinase activity.

To establish the causal relationship between N-MYLK-dependent formation of STIM1 puncta and the SOCE seen in Figure 4 and above, we assessed SOCE in STIM1-depleted EC transducing the N-MYLK mutant. Expression of the N-MYLK mutant in STIM1-depleted EC failed to augment SOCE to the level observed in control cells (Figure 5E-G) recapitulating our findings above that N-MYLK maximizes SOCE by organizing STIM1 puncta at ER-PM junctions.

3.5 | DVRGLL actin-binding motif is required for MYLK-L augmentation of SOCE

Compared to short MYLK isoform, MYLK-L contains two additional motifs which regulate actin remodeling.[22,23] The DVRGV (L)L (V is replaced by L in mouse) located between residues 868-873, and DFRDLL located between residues 895-901 (Figure 6A). We deleted either both motifs or DVRGLL alone in full-length N-MYLK and delineated their roles in mediating SOCE activity (Figure 6A). We observed that the N-MYLK mutant lacking DVRGLL motif (ΔDVRGLL) failed to promote SOCE (Figures 6B,C and S2D), whereas the

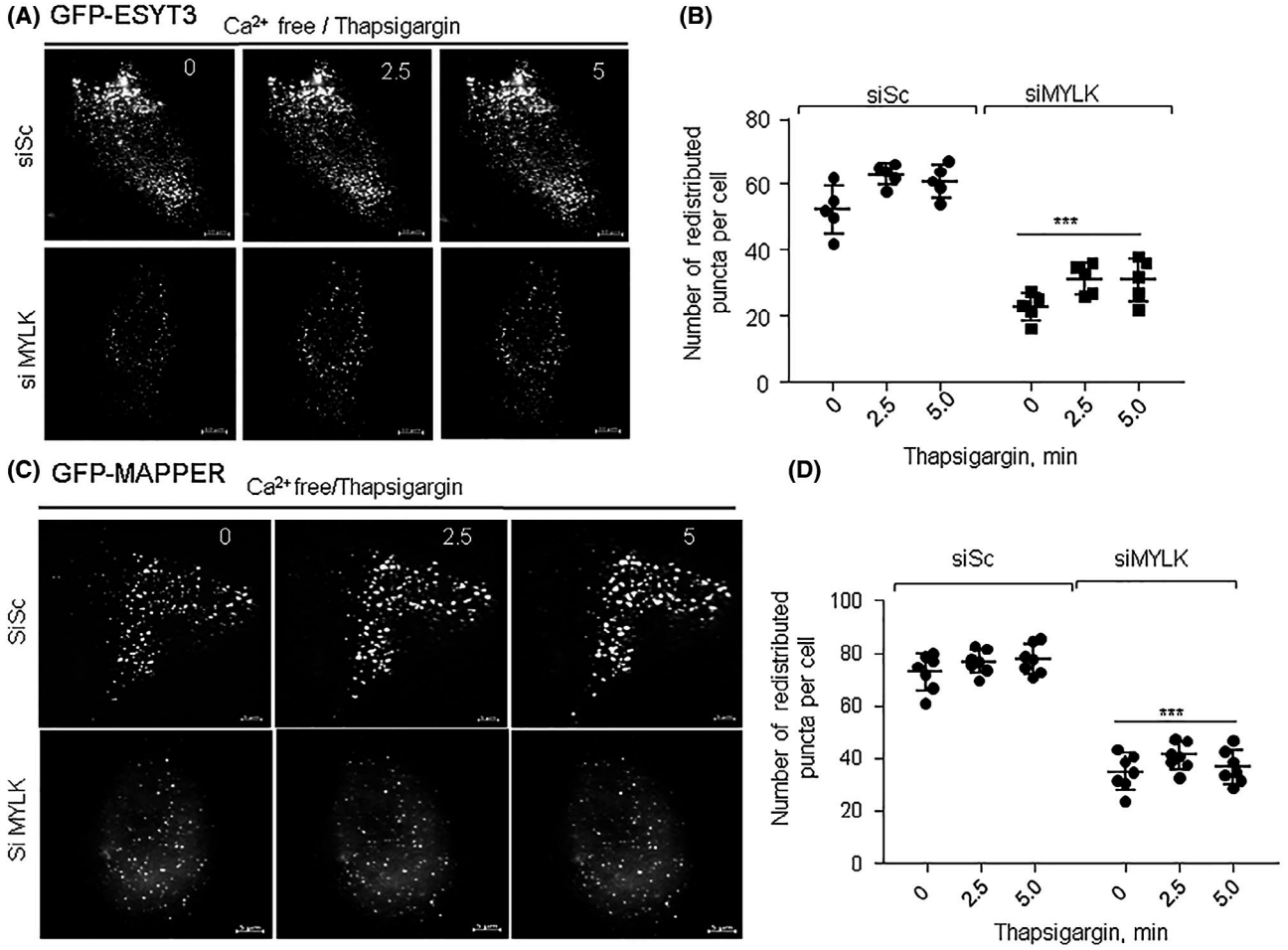

FIGURE 4 MYLK-L promotes store-operated Ca^{2+} entry by stabilizing ER-PM junctions. A and B, Analysis of ER-PM junctions using TIRF live-cell imaging of GFP-ESYT3 in control or MYLK-L-depleted HUVEC before and at different times (min, top right corner) of thapsigargin challenge. Panel A shows a representative image while in B quantification of ER-PM junctions is shown. C and D, Analysis of ER-PM junctions using TIRF live-cell imaging of GFP-MAPPER in control or MYLK-L-depleted HUVEC before and at different times (min, top right corner) of thapsigargin challenge. Panel C shows a representative image while in D quantification of ER-PM junctions is shown. In A and C, the scale bar represents 10 μm. Plot shows mean ± SD of STIM1 puncta or ESYT3 puncta per cell from multiple cells (n > 5) from experiments that were repeated three times. ***, $P < .001$ compared to naïve or thapsigargin stimulated siSc transfected ECs.

N-MYLK mutant lacking both the DVRGLL and DFRDLL motifs (ΔDVRGLL-DFRDLL) did not lead to further decrease in SOCE (Figures 6B,C and S2D). These data indicate that DVRGLL is required for MYLK-L-dependent activation of SOCE. Furthermore, transduction of the ΔDVRGLL-N-MYLK mutant in *MYLK-L*$^{-/-}$EC confirmed the requirement for the DVRGLL motif in activating SOCE (Figures 6D,E and S2E). Deletion of DVRGLL motif from full-length MYLK similarly suppressed SOCE (Figure S2F-H).

3.6 | Transduction of MYLK-L N-terminus domain increases vascular permeability in lungs of *Mylk-L*$^{-/-}$ mice

To address the functional role of SOCE-induced by MYLK-L in regulating endothelial permeability in kinase independent manner, we determined the effect of thapsigargin on MLC phosphorylation and TEER in cells transducing NMYLK or ΔDVRGLL. We found that in control HPAECs thapsigargin-induced MLC-phosphorylation within 2.5 minutes which remains higher than basal level till 5min (Figure S2I). Thapsigargin-induced MLC-phosphorylation was not altered in ECs transducing either NMYLK or ΔDVRGLL (Figure 7A). However, we found that thapsigargin decreased TEER in N-MYLK-L mutant transducing ECs, which did not return to basal value during the 2-hour period (Figure 7B). Interestingly, thapsigargin transiently decreased TEER in ΔDVRGLL transducing ECs, leading to rapid recovery of barrier function within 1 hour (Figure 7B) suggesting that DVRGLL motif-induced SOCE increased endothelial permeability independent of MLC-phosphorylation.

MYLK is a substrate for caspase, which cleaves MYLK into fragments containing active N-terminus.[55] Thus, we used

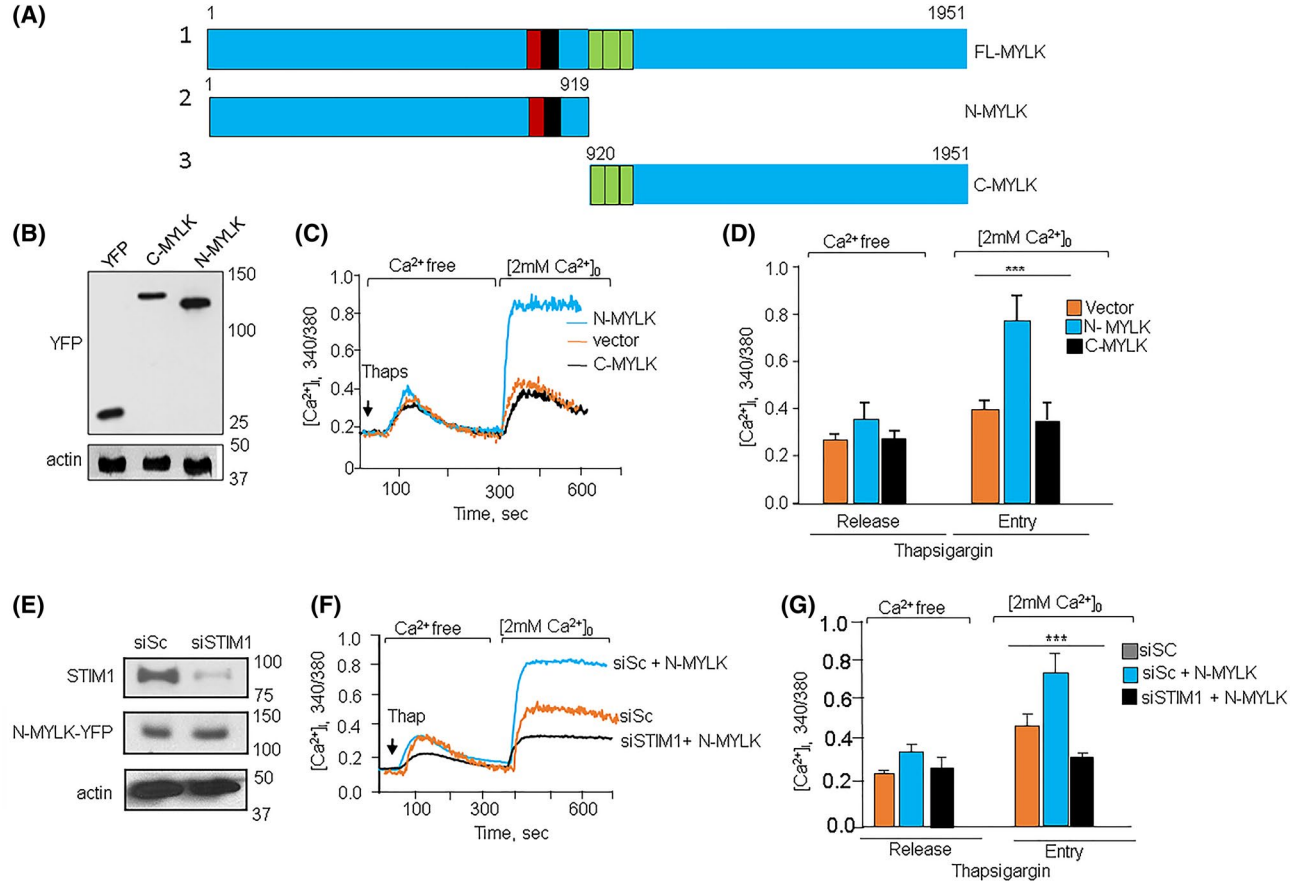

FIGURE 5 N-terminal domain of MLCK-L amplifies and sustains SOC activity. A, Schematic presentation of N- (1-919 aa; N-MYLK) and C- (920-1951 aa; C-MYLK) fragments of MYLK-L (FL-MYLK) cloned into an EYFP vector. B, Immunoblot showing expression of vector (YFP), C- or N-MYLK in HPAEC. HPAEC transducing indicated cDNA were lysed after 24 hours and expression of mutants was assessed using anti-GFP (which also detects YFP expression) antibody. Actin served as a loading control. C and D, Changes in intracellular Ca^{2+} concentration in response to thapsigargin in HPAEC expressing indicated MYLK-L fragments. Panel C shows a representative Fura-2AM 340/380 traces while D shows mean ± SD of intracellular Ca^{2+} 340/380 from 3-4 individual experiments. ***, $P \leq .001$ compared to thapsigargin stimulated vector or C-MYLK expressing HPAEC post addition of 2mM calcium. E, Immunoblot of control or STIM1-depleted HPAEC transducing N-MYLK-L. HPAEC were first transfected with control or STIM1 siRNA. After 24 hours these cells were again transfected with N-MYLK was STIM1 and N-MYLK-L cDNA. Cells were then lysed after 48 hours and expression of indicated cDNA and STIM1 depletion was determined using indicated antibodies; anti-β-actin antibody was used as a loading control. F and G, Changes in intracellular Ca^{2+} concentration in response to thapsigargin in control and STIM1-depleted HPAEC expressing N-MYLK-L cDNA. Panel F shows representative 340/380 Fura2 traces while G shows mean ± SD of data from 3-4 individual experiments. ***, $P \leq .001$ compared to thapsigargin stimulated control ECs or STIM1-depleted EC expressing N-MYLK post addition of 2 mM calcium.

antibody raised against N terminus of MYLK-L to assess if LPS fragmented MYLK-L. LPS-treated lungs showed reduction in the intensity of 210 band and appearance of ~150, 100, 85 kDa fragments not seen in control lungs (Figure S3). One of these fragments corresponds to molecular mass of N-MYLK (100 kDa). Importantly, none of these fragments were absent in naïve or LPS exposed MYLK null lungs (Figure S3). Based on these observations, we assessed if N-MYLK was functional in intact vessels of mice using endotoxin, LPS. We delivered GFP alone, N-MYLK-GFP or the ΔDVRGLL mutants conjugated to liposomes into vasculature of *Mylk-l*$^{-/-}$ mice and exposed these mice to LPS 48 hours later. As expected, LPS failed to increase lung vascular permeability in MYLK-L null mice transducing the GFP vector. However, transduction of N-MYLK *but not* the ΔDVRGLL-N-MYLK mutant in MYLK-L null mice restored lung vascular permeability in response to LPS to the level observed in WT mice (Figure 7C,D), suggesting that N-MYLK alone contributes to vascular leakage by activating SOCE.

4 | DISCUSSION

Besides the catalytic domain that regulates the endothelial contractility MYLK-L contains an N-terminal domain of unknown function. Our study showed that the N-terminus

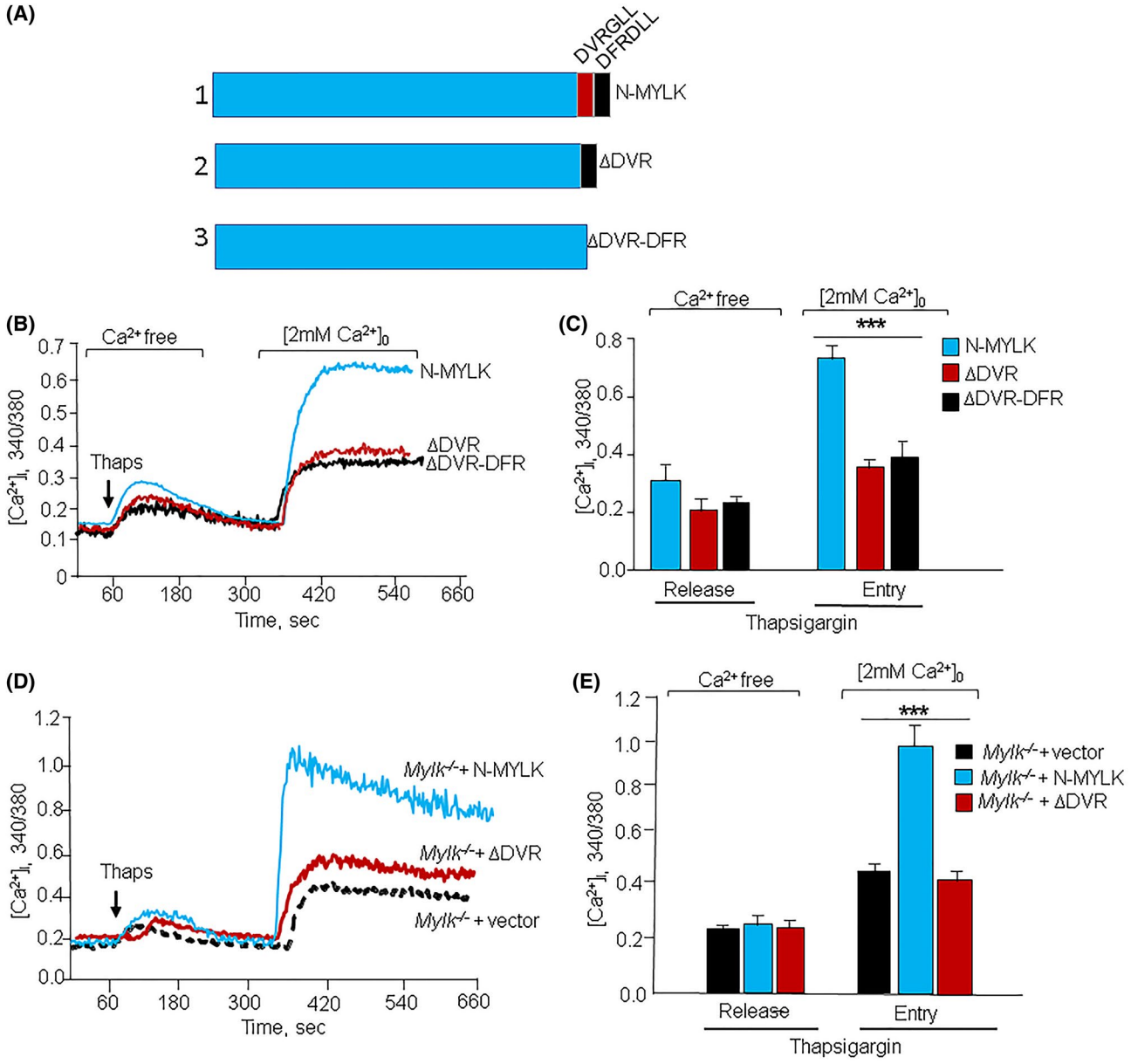

FIGURE 6 MYLK-L promotes SOCE through DVRGLL actin-binding motif. A, Schematic representation of N-MYLK-L mutant or mutants lacking one (ΔDVRGLL) or two (ΔDVRGLL-DFRDLL) actin-binding motifs. B and C, Changes in intracellular Ca^{2+} concentration in response to thapsigargin in HPAEC expressing indicated mutants. Panel B shows representative Fura-2AM 340/380 traces while C shows mean ± SD from 3-4 individual experiments. ***, $P \leq .001$ compared to thapsigargin stimulated ΔDVRGLL or ΔDVRGLL-DFRDLL mutant expressing HPAECs post addition of 2mM calcium addition. D and E, Changes in intracellular Ca^{2+} concentration in response to thapsigargin in *Mylk*$^{-/-}$ lung EC expressing either ΔDVRGLL-N-MYLK or N-MYLK mutants. Panel D shows representative Fura-2AM 340/380 traces while E shows mean ± SD from 3-4 individual dishes. ***, $P \leq .001$ compared to thapsigargin stimulated vector or ΔDVRGLL mutant expressing MYLK-L null EC post addition of 2mM calcium addition.

of MYLK-L promoted SOCE independent of the catalytic activity of the enzyme. We also demonstrated a novel role of the "DVRGLL" motif located within the N-terminus in inducing pulmonary edema in response to LPS. We showed that the DVRGLL motif within the N-terminus of MYLK-L increases ER-PM junctions enabling STIM1 puncta translocation to these junctions and thereby augmentation of SOCE and lung injury.

MYLK-L belongs to the family of Ca^{2+}-calmodulin-dependent kinases. Under basal conditions, MYLK is auto-inhibited due to interaction of basic residues within the inhibitory domain of the enzyme with the acidic residues within the catalytic core.[56] A rise in cytosolic Ca^{2+} and calmodulin binding is required for conformational changes enabling activation of MYLK-L kinase and MLC phosphorylation which in turn can increase endothelial

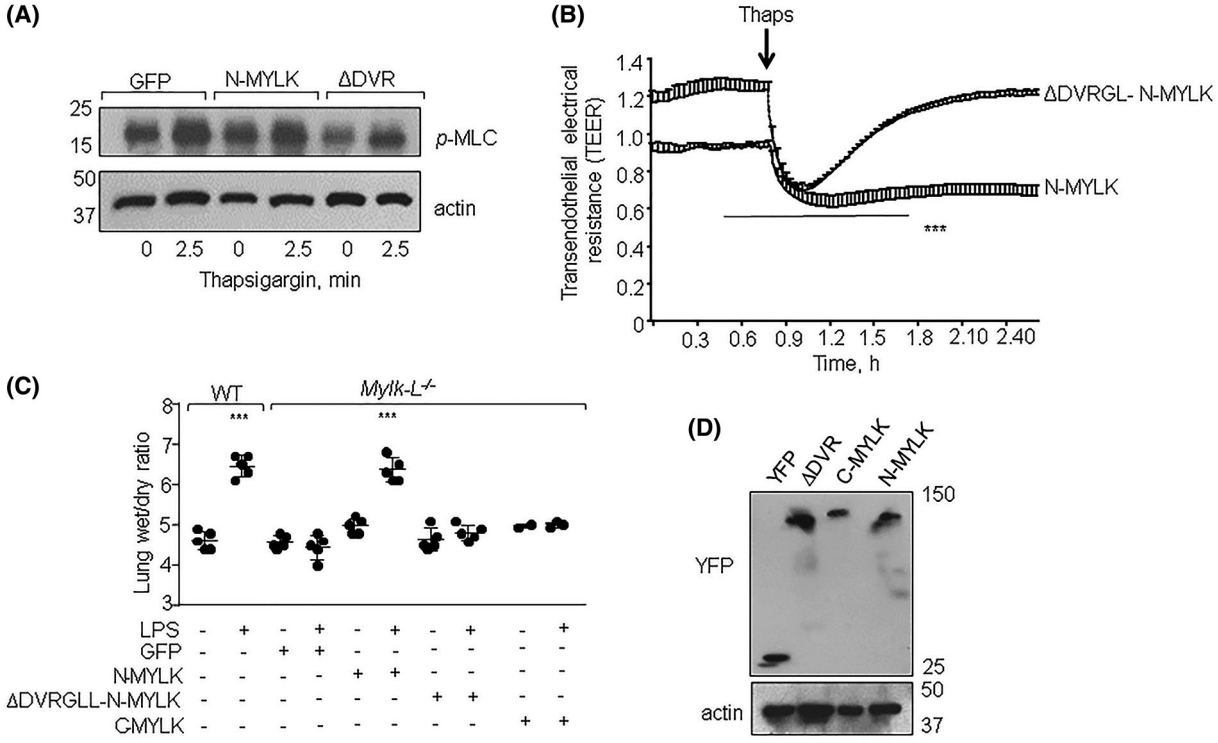

FIGURE 7 N-MYLK rescues lung vascular permeability. A and B, HPAEC were transduced either with vector, NMYLK or ΔDVRGLL-N-MYLK mutants and plated on either six well plates or TEER electrodes. After 24 hours, MLC phosphorylation (A) or endothelial barrier function (TEER) (B) was determined following stimulation with thapsigargin. MLC phosphorylation was determined using phosphor-MLC antibody at indicated times. Actin was used as a loading control. Data show mean ± SD from 3-4 individual experiments. ***, $P \leq .001$ compared to ΔDVRGLL-N-MYLK mutant expressing HPAEC. C and D, Pulmonary edema in *Mylk-L*$^{-/-}$ mice expressing YFP, N-MYLK, or ΔDVRGLL-N-MYLK mutant following LPS exposure. (B) Immunoblot analysis with anti-GFP antibody shows expression of indicated mutants in lung EC. EC ($CD31^+/CD45^-$) were flow-sorted from lungs of mice expressing indicated mutants. n = 5 mice per group). ***, $P \leq .001$ compared to unexposed WT mice or MYLK null mice expressing indicated cDNA after without or with LPS challenge.

permeability.[30,31,49,57] The findings of the current studies revealed a novel kinase-independent function of MYLK-L in regulating SOCE and Ca^{2+} signaling in ECs. This function of MYLK-L required the unique N-terminal domain of MYLK-L. The ectopic expression of N-MYLK-L mutant markedly enhanced SOCE in ECs, whereas overexpression of the C-MYLK mutant (similar to short isoform of MYLK) had no effect even though C-MYLK mutant increased MLC phosphorylation. Furthermore, transduction of an N-MYLK mutant in MYLK-L deficient EC but not ΔDVRGLL-N-MYLK mutant promoted SOCE to the level observed in WT-EC. We also showed that N-MYLK mutant increased SOCE and endothelial permeability without altering the increase in MLC-phosphorylation. Further studies showed that loss of MYLK-L impaired vascular permeability responses to permeability increasing mediators such as thrombin and endotoxin as well as thapsigargin, consistent with published studies.[6,16,17,19] A caveat is that these studies do not rule out if MYLK-L from other cell types compensated in regulating vascular permeability since Tie2-cre-mediated deletion of MYLK-L in mice did not alter LPS-induced lung vascular permeability.[20] However, we showed that transduction of N-MYLK but not ΔDVRGLL-N-MYLK mutant in MYLK-null mice rescued lung edema formation by LPS. Thus, our findings suggest that MYLK-L maximizes SOCE via the N-terminus domain leading to disruption of the EC barrier.

Activation of SOCE requires coordinated integration between multiple pathways.[31-34] Upon depletion of ER stores, STIM1 forms puncta that are redistributed to the ER-PM junctions for targeted activation of Orai1 and TRPC1/4 channels at the PM. In this context, several proteins including CRACR2A, STIMATE, SARAF, septins, and RASSF4 are known to regulate SOCE by regulating the STIM1 activity.[51,58-60] Whereas STIM1 puncta formation may be modulated by posttranslational modifications of STIM1[44,61-63] our findings demonstrated that the N-MYLK mutant, which lacks kinase activity, promoted SOCE in MYLK deficient EC, ruling out the role of MYLK enzymatic activity in regulating STIM1 puncta. Notably, we showed MYLK-L functioned by forming ER-PM junctions since formation of all MAPPER- and E-SYT 3-positive ER-PM junctions were significantly compromised in MYLK-L-depleted cells. We speculate

that through this function MYLK-L enables STIM1 redistribution to PM followed by protracted SOCE influx under inflammatory conditions. While ER-PM junctions are not completely lost in MYLK-L-depleted ECs, these junctions are not sufficient for maximal STIM1 activation of SOCE. We also showed that N-MYLK failed to rescue SOCE in STIM1-depleted ECs demonstrating the STIM1 requirement for MYLK-L-dependent regulation of SOCE. Thus, our findings demonstrate that MYLK-L has a crucial role in enhancing SOCE and does so by stabilizing ER-PM junctions and STIM1 redistribution at these junctions.

How DVRGLL motif in MYLK-N-terminus increased ER-PM junctions needs to parse out but some speculations can be made. Actin cytoskeletal remodeling can promote anchoring of subcellular organelles including the ER to the PM,[43,64-66] which we surmise can promote ER-PM junction formation. Consistent with this concept, we showed that the actin-binding DVRGLL motif located in the N-terminal domain of MYLK-L is required for maximal SOCE. We showed that loss of the DVRGLL motif caused significant impairment of SOCE upon thapsigargin stimulation, in agreement with the proposed role of MYLK-L in EC. In addition, N-MYLK but not N-MYLK lacking DVRGLL rescued full activation of SOCE in EC isolated from *Mylk-l*$^{-/-}$ lungs. These findings suggest that the DVRGLL motif within MYLK-L serves as a scaffold to locally organize actin cytoskeleton remodeling at the sites of ER-PM junctions enabling distribution of STIM1 puncta and associated activation of SOCE. It is also possible that the DVRGLL may function via other actin crosslinking proteins such as filamin-A, which is known to facilitate STIM1 ER-PM junctions and thereby SOCE[66-68]

Studies show that caspases activated upon vascular injury cleaves MYLK-L into smaller constitutively active MYLK fragments.[55] We showed that LPS-induced MYLK-L cleavage leading to generation of several N-terminus containing MYLK-L fragments including one which corresponds to N-MYLK-L in molecular mass. Further, we established here the critical role of the DVRGLL motif of N-MYLK-L in disrupting endothelial barrier function by enhancing SOCE. Strikingly, we showed that liposomal delivery of N-MYLK increased vascular permeability in MYLK-L null mice and this function of MYLK-L required an intact DVRGLL-motif. Adherens junctions (AJ) formed via complexes of VE-cadherin and associated catenin proteins are required to establish the endothelial barrier.[1-3] It is also known that SOCE can directly influence AJ via posttranslational modification of β- and p120-catenin proteins or VE-cadherin through tyrosine and serine/threonine kinases such as Src, protein kinase C, Rho kinase, and Src.[1-3] Thus, it is possible that N-MYLK-induced SOCE increases vascular permeability by altering the phosphorylation status of constituents of AJs.

Taken together, our data for the first time describe the heretofore unknown function of the actin-binding motif within the N-terminal domain of MYLK-L in regulating vascular permeability by augmenting SOCE through the formation of STIM1 puncta at ER-PM junctions. Our studies indicate that N-terminal domain reported here maximizes the increase in vascular permeability by placing Ca^{2+} entry upstream of actin-myosin contraction. In this sense, the DVRGLL motif in MYLK-L represents a novel target for treating vascular leak disorders such as ALI without compromising the contractile function of ECs.

ACKNOWLEDGMENTS

The authors acknowledge Drs. H Piplani and Peter Toth for their technical support. M. Watterson (Department of Molecular Biology and Biochemistry and Pharmacology, Northwestern University, Chicago, IL) for providing *Mylk-L*$^{-/-}$ knockout mouse, Dr Patricia Gallagher (Department of Physiology, School of Medicine, Indiana University) for providing GFP-tagged mouse MYLK-L (WT-MYLK-L) plasmid and Dr Jen Liou (Department of Physiology, University of Texas Southwestern Medical Center) for providing STIM1; YFP-MAPPER and YFP-ESYT-3 plasmids. This work was supported by NIH grants HL84153, HL137179-01, PO1-HL60678, and HL077806.

CONFLICT OF INTEREST

The authors declare no competing interests.

AUTHOR CONTRIBUTIONS

N. Srivastava and D. Mehta designed the research; N. Srivastava, M. Tauseef, R. MD-R Amin, B. Joshi, JC Joshi, V. Kini, J. Klomp, W. Li, N. Knezevic, N. Barbera, and A. A Obukhov, performed the experiments; A. Karginov, I. Levitan, and S. Siddiqui contributed new reagents; N. Srivastava, M. Tauseef, MD-R Amin, and Y. Komarova analyzed the data and commented on manuscript; N. Srivastava and D. Mehta wrote the manuscript.

REFERENCES

1. Dudek SM, Garcia JG. Cytoskeletal regulation of pulmonary vascular permeability. *J Appl Physiol (1985)*. 2001;91:1487-1500.
2. Mehta D, Malik AB. Signaling mechanisms regulating endothelial permeability. *Physiol Rev*. 2006;86:279-367.
3. Komarova YA, Kruse K, Mehta D, Malik AB. Protein interactions at endothelial junctions and signaling mechanisms regulating endothelial permeability. *Circ Res*. 2017;120:179-206.
4. Mehta D, Bhattacharya J, Matthay MA, Malik AB. Integrated control of lung fluid balance. *Am J Physiol Lung Cell Mol Physiol*. 2004;287:L1081-L1090.
5. Shen Q, Rigor RR, Pivetti CD, Wu MH, Yuan SY. Myosin light chain kinase in microvascular endothelial barrier function. *Cardiovasc Res*. 2010;87:272-280.

6. Sun C, Wu MH, Yuan SY. Nonmuscle myosin light-chain kinase deficiency attenuates atherosclerosis in apolipoprotein E–deficient mice via reduced endothelial barrier dysfunction and monocyte migration. *Circulation*. 2011;124:48-57.
7. Matthay MA, Zemans RL. The acute respiratory distress syndrome: pathogenesis and treatment. *Annu Rev Pathol*. 2011;6:147-163.
8. Garcia J, Lazar V, Gilbert-McClain LI, Gallagher PJ, Verin AD. Myosin light chain kinase in endothelium: molecular cloning and regulation. *Am J Respir Cell Mol Biol*. 1997;16:489-494.
9. Verin AD, Gilbert-McClain LI, Patterson CE, Garcia JG. Biochemical regulation of the nonmuscle myosin light chain kinase isoform in bovine endothelium. *Am J Respir Cell Mol Biol*. 1998;19:767-776.
10. Blue EK, Goeckeler ZM, Jin Y, et al. 220-and 130-kDa MLCKs have distinct tissue distributions and intracellular localization patterns. *Am J Physiol Cell Physiol*. 2002;282:C451-C460.
11. Goeckeler ZM, Wysolmerski RB. Myosin light chain kinase-regulated endothelial cell contraction: the relationship between isometric tension, actin polymerization, and myosin phosphorylation. *J Cell Biol*. 1995;130:613-627.
12. Wysolmerski RB, Lagunoff D. Involvement of myosin light-chain kinase in endothelial cell retraction. *Proc Natl Acad Sci USA*. 1990;87:16-20.
13. Yuan Y, Huang Q, Wu HM. Myosin light chain phosphorylation: modulation of basal and agonist-stimulated venular permeability. *Am J Physiol*. 1997;272:H1437-H1443.
14. Tinsley JH, De Lanerolle P, Wilson E, Ma W, Yuan SY. Myosin light chain kinase transference induces myosin light chain activation and endothelial hyperpermeability. *Am J Physiol Cell Physiol*. 2000;279:C1285-C1289.
15. Bogatcheva NV, Zemskova MA, Poirier C, et al. The suppression of myosin light chain (MLC) phosphorylation during the response to lipopolysaccharide (LPS): beneficial or detrimental to endothelial barrier? *J Cell Physiol*. 2011;226:3132-3146.
16. Wainwright MS, Rossi J, Schavocky J, et al. Protein kinase involved in lung injury susceptibility: evidence from enzyme isoform genetic knockout and in vivo inhibitor treatment. *Proc Natl Acad Sci USA*. 2003;100:6233-6238.
17. Rossi JL, Velentza AV, Steinhorn DM, Watterson DM, Wainwright MS. MLCK210 gene knockout or kinase inhibition preserves lung function following endotoxin-induced lung injury in mice. *Am J Physiol Lung Cell Mol Physiol*. 2007;292:L1327-L1334.
18. Xu J, Gao X-P, Ramchandran R, Zhao Y-Y, Vogel SM, Malik AB. Nonmuscle myosin light-chain kinase mediates neutrophil transmigration in sepsis-induced lung inflammation by activating Î2 2 integrins. *Nat Immunol*. 2008;9:880.
19. Reynoso R, Perrin RM, Breslin JW, et al. A role for long chain myosin light chain kinase (MLCK-210) in microvascular hyperpermeability during severe burns. *J Shock*. 2007;28:589-595.
20. Yu Y, Lv N, Lu Z, et al. Deletion of myosin light chain kinase in endothelial cells has a minor effect on the lipopolysaccharide-induced increase in microvascular endothelium permeability in mice. *FEBS J*. 2012;279:1485-1494.
21. Birukov KG, Csortos C, Marzilli L, et al. Differential regulation of alternatively spliced endothelial cell myosin light chain kinase isoforms by p60Src. *J Biol Chem*. 2001;276:8567-8573.
22. Kudryashov DS, Chibalina MV, Birukov KG, et al. Unique sequence of a high molecular weight myosin light chain kinase is involved in interaction with actin cytoskeleton. *FEBS Lett*. 1999;463:67-71.
23. Kudryashov DS, Stepanova OV, Vilitkevich EL, et al. Myosin light chain kinase (210 kDa) is a potential cytoskeleton integrator through its unique N-terminal domain. *Exp Cell Res*. 2004;298:407-417.
24. Gao L, Grant A, Halder I, et al. Novel polymorphisms in the myosin light chain kinase gene confer risk for acute lung injury. *Am J Respir Cell Mol Biol*. 2006;34:487-495.
25. Gao L, Grant AV, Rafaels N, et al. Polymorphisms in the myosin light chain kinase gene that confer risk of severe sepsis are associated with a lower risk of asthma. *J Allergy Clin Immunol*. 2007;119:1111-1118.
26. Christie JD, Ma S-F, Aplenc R, et al. Variation in the myosin light chain kinase gene is associated with development of acute lung injury after major trauma. *Crit Care Med*. 2008;36:2794-2800.
27. Wu MM, Buchanan J, Luik RM, Lewis RS. Ca^{2+} store depletion causes STIM1 to accumulate in ER regions closely associated with the plasma membrane. *J Cell Biol*. 2006;174:803-813.
28. Tauseef M, Knezevic N, Chava KR, et al. TLR4 activation of TRPC6-dependent calcium signaling mediates endotoxin-induced lung vascular permeability and inflammation. *J Exp Med*. 2012;209:1953-1968.
29. Tauseef M, Farazuddin M, Sukriti S, et al. Transient receptor potential channel 1 maintains adherens junction plasticity by suppressing sphingosine kinase 1 expression to induce endothelial hyperpermeability. *FASEB J*. 2016;30:102-110.
30. Townsley MI. Permeability and calcium signaling in lung endothelium: unpack the box…. *Pulm Circ*. 2017;8. https://doi.org/10.1177/2045893217738218.
31. Tiruppathi C, Freichel M, Vogel SM, et al. Impairment of store-operated Ca2+ entry in TRPC4(-/-) mice interferes with increase in lung microvascular permeability. *Circ Res*. 2002;91:70-76.
32. Cahalan MD. STIMulating store-operated Ca 2+ entry. *Nat Cell Biol*. 2009;11:669.
33. Smyth JT, Hwang SY, Tomita T, DeHaven WI, Mercer JC, Putney JW. Activation and regulation of store-operated calcium entry. *J Cell Mol Med*. 2010;14:2337-2349.
34. Prakriya M, Lewis RS. Store-operated calcium channels. *Physiol Rev*. 2015;95:1383-1436.
35. Liou J, Kim ML, Do Heo W, et al. STIM is a Ca^{2+} sensor essential for Ca^{2+}-store-depletion-triggered Ca^{2+} influx. *Curr Biol*. 2005;15:1235-1241.
36. Soboloff J, Rothberg BS, Madesh M, Gill DL. STIM proteins: dynamic calcium signal transducers. *Nat Rev Mol Cell Biol*. 2012;13:549–565.
37. Zhou Y, Srinivasan P, Razavi S, et al. Initial activation of STIM1, the regulator of store-operated calcium entry. *Nat Struct Mol Biol*. 2013;20:973-981.
38. Muallem S, Jha A. Opening the Orai1 gates. *Sci Signal*. 2017;10:eaaq0618.
39. Ong HL, , . STIM-TRP pathways and microdomain organization: contribution of TRPC1 in store-operated Ca^{2+} entry: impact on Ca^{2+} signaling and cell function, , . In *Store-operated Ca2⁺ entry (SOCE) pathways*. New York, NY: Springer; 2017:159-188.
40. Smyth JT, DeHaven WI, Bird GS, Putney JW. Ca^{2+}-store-dependent and-independent reversal of Stim1 localization and function. *J Cell Sci*. 2008;121:762-772.
41. Knezevic N, Tauseef M, Thennes T, Mehta D. The G protein betagamma subunit mediates reannealing of adherens junctions to reverse endothelial permeability increase by thrombin. *J Exp Med*. 2009;206:2761-2777.

42. Liou J, Fivaz M, Inoue T, Meyer T. Live-cell imaging reveals sequential oligomerization and local plasma membrane targeting of stromal interaction molecule 1 after Ca^{2+} store depletion. *Proc Natl Acad Sci*. 2007;104:9301-9306.
43. Hsieh T-S, Chen Y-J, Chang C-L, Lee W-R, Liou JJM. Cortical actin contributes to spatial organization of ER–PM junctions. *J Mol Biol Cell*. 2017;28:3171-3180.
44. Yazbeck P, Tauseef M, Kruse K, et al. STIM1 phosphorylation at Y361 recruits Orai1 to STIM1 puncta and induces Ca^{2+} entry. *Sci Rep*. 2017;7:42758.
45. Edelstein A, Amodaj N, Hoover K, Vale R, Stuurman N. Computer control of microscopes using μManager. *Curr Prot Mol Biol*. 2010;92:14.20. 11-14.20. 17.
46. Wu S, Sangerman J, Li M, Brough GH, Goodman SR, Stevens T. Essential control of an endothelial cell ISOC by the spectrin membrane skeleton. *J Cell Biol*. 2001;154:1225-1233.
47. Singh I, Knezevic N, Ahmmed GU, Kini V, Malik AB, Mehta D. Galphaq-TRPC6-mediated Ca2+ entry induces RhoA activation and resultant endothelial cell shape change in response to thrombin. *J Biol Chem*. 2007;282:7833-7843.
48. Kini V, Chavez A, Mehta D. A new role for PTEN in regulating transient receptor potential canonical channel 6-mediated Ca2+ entry, endothelial permeability, and angiogenesis. *J Biol Chem*. 2010;285:33082-33091.
49. Wu S, Cioffi EA, Alvarez D, et al. Essential role of a Ca^{2+}-selective, store-operated current (ISOC) in endothelial cell permeability: determinants of the vascular leak site. *Circ Res*. 2005;96:856-863.
50. Gandhirajan RK, Meng S, Chandramoorthy HC, et al. Blockade of NOX2 and STIM1 signaling limits lipopolysaccharide-induced vascular inflammation. *J Clin Investig*. 2013;123:887–902.
51. Chen Y-J, Chang C-L, Lee W-R, Liou J. RASSF4 controls SOCE and ER–PM junctions through regulation of PI(4,5)P2. *J Cell Biol*. 2017;216:2011-2025. https://doi.org/10.1083/jcb.201606047.
52. Steyer JA, Almers W. A real-time view of life within 100 nm of the plasma membrane. *Nat Rev Mol Cell Biol*. 2001;2:268.
53. Chang C-L, Hsieh T-S, Yang TT, et al. Feedback regulation of receptor-induced Ca^{2+} signaling mediated by E-Syt1 and Nir2 at endoplasmic reticulum-plasma membrane junctions. *Cell Rep*. 2013;5:813-825.
54. Giordano F, Saheki Y, Idevall-Hagren O, et al. PI (4, 5) P2-dependent and Ca^{2+}-regulated ER-PM interactions mediated by the extended synaptotagmins. *Cell*. 2013;153:1494-1509.
55. Petrache I, Birukov K, Zaiman AL, et al. Caspase-dependent cleavage of myosin light chain kinase (MLCK) is involved in TNF-α-mediated bovine pulmonary endothelial cell apoptosis. *FASEB J*. 2003;17:407-416.
56. Gallagher PJ, Herring BP, Trafny A, Sowadski J, Stull JT. A molecular mechanism for autoinhibition of myosin light chain kinases. *J Biol Chem*. 1993;268:26578-26582.
57. Stolwijk JA, Zhang X, Gueguinou M, et al. Calcium signaling is dispensable for receptor regulation of endothelial barrier function. *J Biol Chem*. 2016;291:22894-22912.
58. Srikanth S, Gwack Y. Orai1, STIM1, and their associating partners. *J Physiol*. 2012;590:4169-4177.
59. Palty R, Raveh A, Kaminsky I, Meller R, Reuveny E. SARAF inactivates the store operated calcium entry machinery to prevent excess calcium refilling. *Cell*. 2012;149:425-438.
60. Jing JI, He L, Sun A, et al. Proteomic mapping of ER–PM junctions identifies STIMATE as a regulator of Ca 2+ influx. *Nat Cell Biol*. 2015;17:1339.
61. Smyth JT, Petranka JG, Boyles RR, et al. Phosphorylation of STIM1 underlies suppression of store-operated calcium entry during mitosis. *Nat Cell Biol*. 2009;11:1465.
62. Pozo-Guisado E, Casas-Rua V, Tomas-Martin P, Lopez-Guerrero AM, Alvarez-Barrientos A, Martin-Romero FJ. Phosphorylation of STIM1 at ERK1/2 target sites regulates interaction with the microtubule plus-end binding protein EB1. *J Cell Sci*. 2013;126:3170-3180.
63. Casas-Rua V, Tomas-Martin P, Lopez-Guerrero AM, Alvarez IS, Pozo-Guisado E, Martin-Romero FJ. STIM1 phosphorylation triggered by epidermal growth factor mediates cell migration. *Biochim Biophys Acta – Mol Cell Res*. 2015;1853:233-243.
64. Rosado JA, Sage SO. The actin cytoskeleton in store-mediated calcium entry. *J Physiol*. 2000;526(Pt 2):221-229.
65. Rosado JA, Jenner S, Sage SO. A role for the actin cytoskeleton in the initiation and maintenance of store-mediated calcium entry in human platelets Evidence for conformational coupling. *J Biol Chem*. 2000;275:7527-7533.
66. van Vliet AR, Agostinis PJM. PERK and filamin A in actin cytoskeleton remodeling at ER-plasma membrane contact sites. *Mol Cell Oncol*. 2017;4:e1340105.
67. Lynch CD, Sheetz MP. Cellular mechanotransduction: filamin A strains to regulate motility. *Curr Biol*. 2011;21:R916-R918.
68. Lynch CD, Gauthier NC, Biais N, et al. Filamin depletion blocks endoplasmic spreading and destabilizes force-bearing adhesions. *Mol Biol Cell*. 2011;22:1263-1273.

SUPPORTING INFORMATION

Additional supporting information may be found online in the Supporting Information section.

How to cite this article: Srivastava NN, Tauseef M, Amin R, et al. Noncanonical function of long myosin light chain kinase in increasing ER-PM junctions and augmentation of SOCE. *The FASEB Journal*. 2020;34:12805–12819. https://doi.org/10.1096/fj.201902462RR